Orographic Drag Parameterization History and Issues

N. McFarlane

CCCma/University of Victoria

OUTLINE

- Historical Overview
  - Early papers concerning orographic gravity-wave drag processes
  - Early operational implementations of orographic gravity-wave drag (OGWD) parameterization schemes in NWP models and GCMs

- Other drag processes
  - Downslope wind effects
  - Blocking

- Issues

J. S. Sawyer, QJRMS, 1959:
The introduction of the effects of topography into methods of numerical forecasting

"The motions which are caused directly by topography may be classified broadly as:
(a) Small-scale turbulent motion mainly in the lower troposphere.
(b) Gravity oscillations which may extend upwards as far as the stratosphere.
(c) Oscillations about geostrophic equilibrium.
(d) Quasi-geostrophic motions."

- Derives an expression for the surface drag due to upward propagating gravity-waves generation by flow over a bell-shaped ridge following the treatment of Scorer (1949), (but with the upper boundary condition proposed by Corby& Sawyer, 1958).

"*… If the ridges are spaced at intervals of 10 km the average drag is 7.6 dyne cm^{-2} which is about the same as the frictional drag over ordinary terrain in a similar wind.*
… A rough approximation to the effect on the atmosphere of the drag from gravity-type disturbances would thus be provided by introducing into the equations of motion a force in the opposite direction to the low-level wind and decreasing linearly from a maximum near the ground to zero at the tropopause."

[Discussed including effects on the large-scale vorticity fields in the the quasi-geostrophic two-parameter model of Sawyer and Bushby (1953)]

G. P. Cressman, MWR, 1960: IMPROVED TERRAIN EFFECTS IN BAROTROPIC FORECASTS

- Considers the contribution of mountain drag in constructing a bulk drag coefficient for use in barotropic forecast models.

"*In order to incorporate friction into the forecast in any scale of motion smaller than the zonal vortex itself, it is necessary to have a map of the distribution of the drag coefficient over the forecast area,…*"

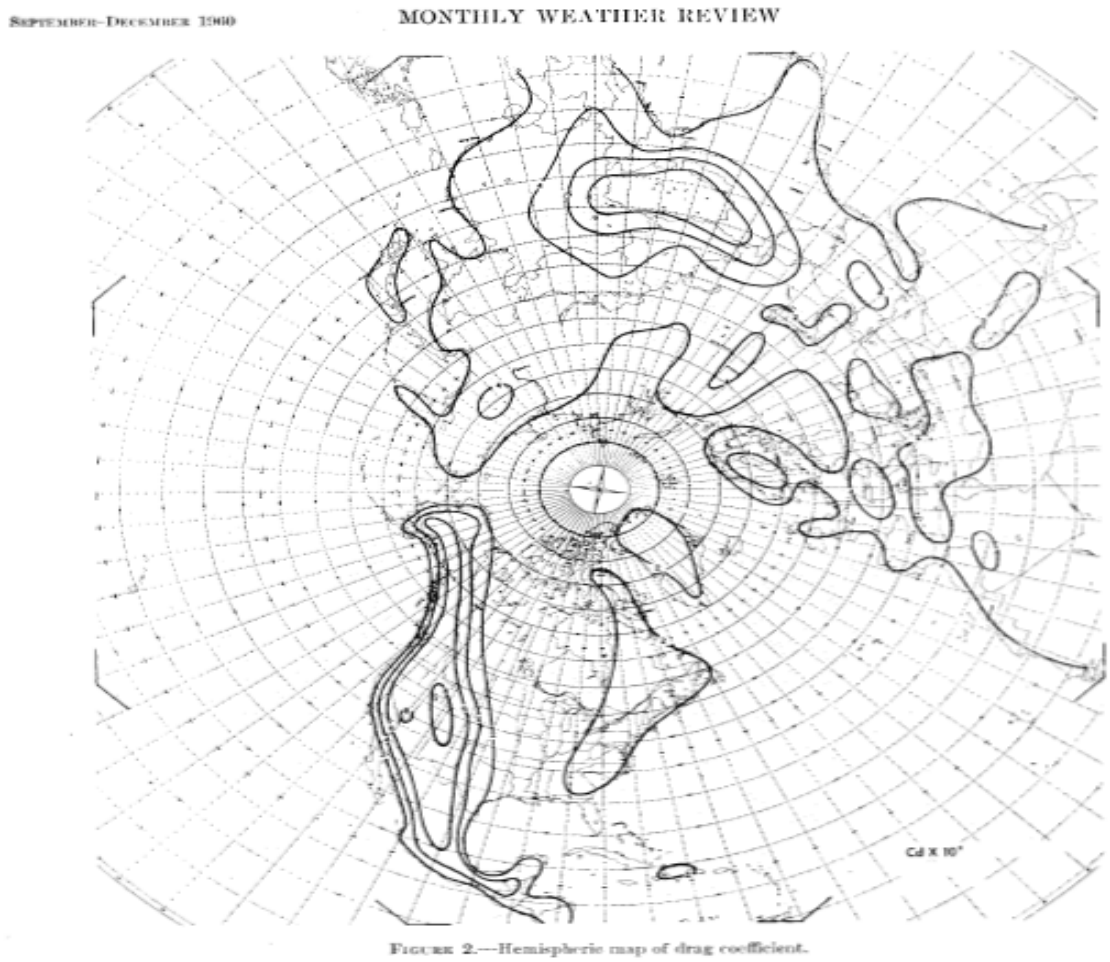

FIGURE 2.—Hemispheric map of drag coefficient.

Contours : 2×10^{-3}

Motivation for introducing gravity-wave drag parameterizations in operational NWP models and GCMs (in the late 1980s and later).

- With the advent of operational multi-level PE models for medium range forecasting and climate simulation, a number of systematic errors in the representation of large-scale flow features became apparent.
- Errors in the magnitude and vertical structure of zonal mean winds in the extra-tropics were among the more robust of these.

In particular:

(a) the mean zonal winds in mid-latitudes in the troposhere were typically too strong and the jet streams were not realistically closed.

(b) the associated surface pressure and geopotential height (temperature) fields had low (cold) biases over polar regions, particularly in the Northern Hemisphere winter.

- These biases were not substantially alleviated by increasing the spatial (horizontal) resolution to the extent operationally feasible.

Palmer et al., 1986

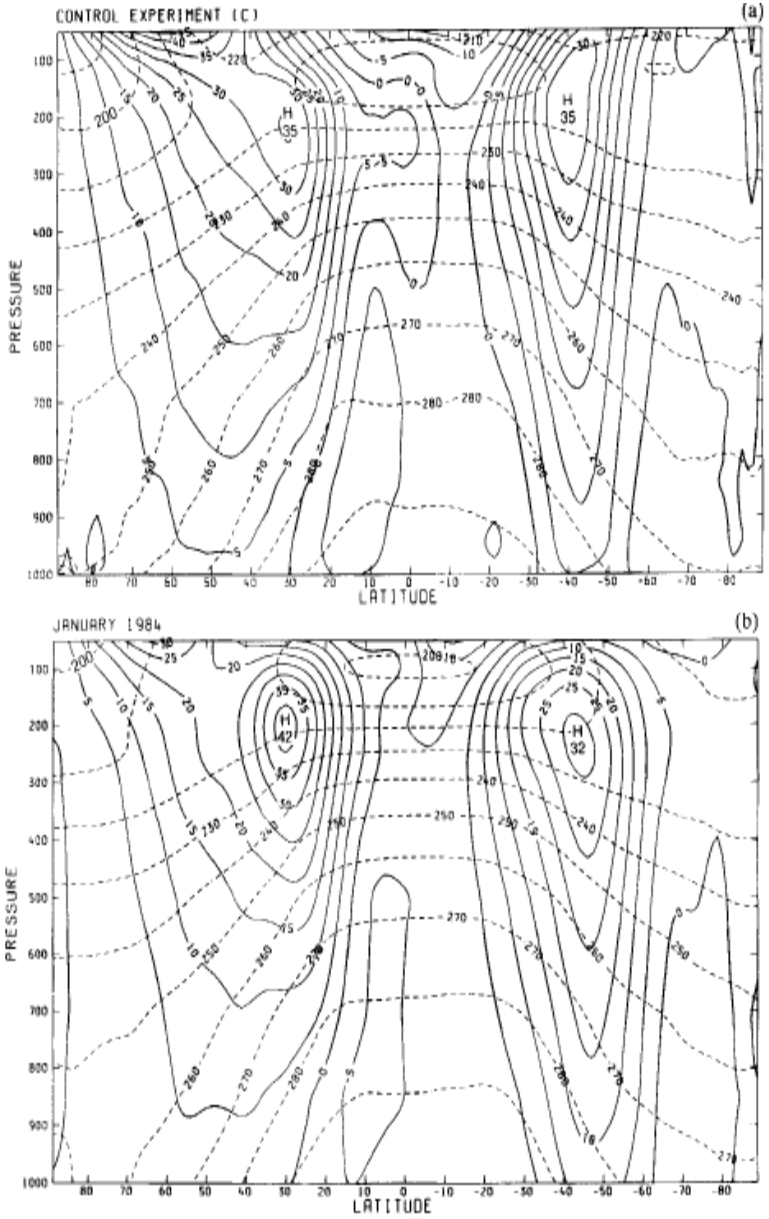

Figure 2. Zonal mean cross-sections of zonal wind ($m\,s^{-1}$) and temperature (K, dashed lines) for (a) days 31–90 of a January integration of the Meteorological Office 11-layer GCM (experiment C—see section 6); (b) January 1984, as derived from the Meteorological Office operational analyses.

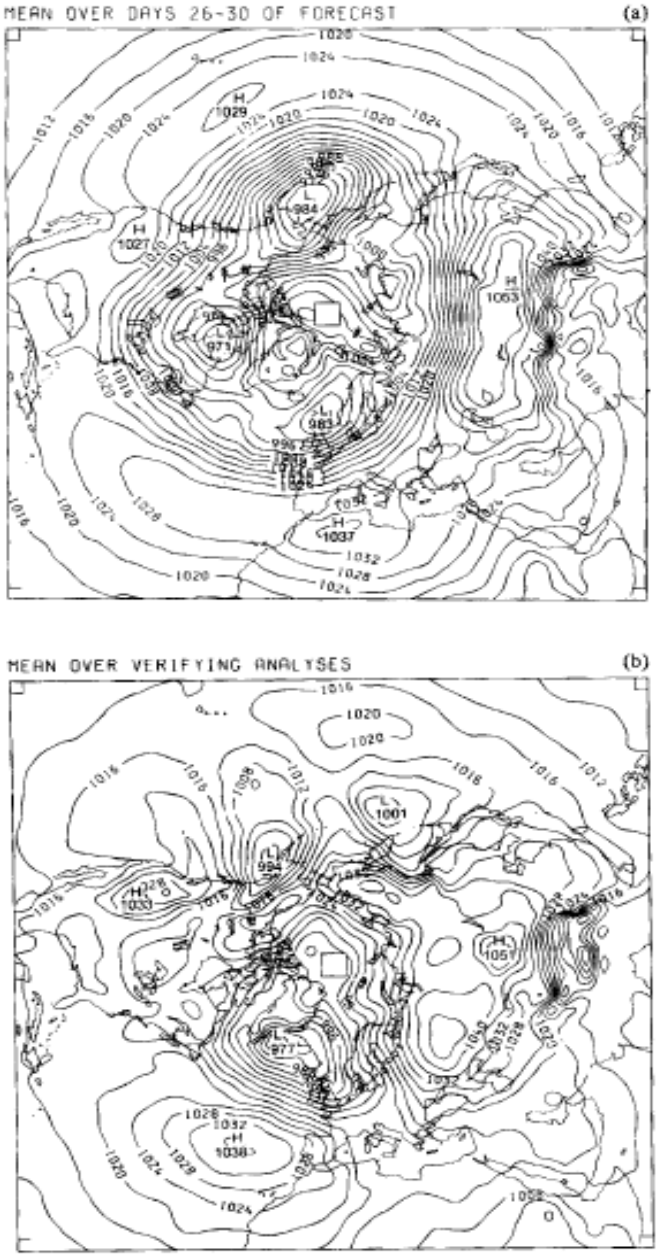

Figure 1. (a) Time-mean sea level pressure field from days 26–30 of a wintertime forecast with the Meteorological Office operational model (prior to the inclusion of gravity wave drag). (b) The verifying analysis.

Key Theoretical Advances

- **Eliasen and Palm** (1960) – In the absence of transience and dissipation the vertical momentum flux is independent of height for vertically propagating gravity-waves .

- **Booker and Bretherton** (1967) – critical layer absorption [exponential damping of upward propagating GW at critical levels in stable stratification ($Ri_c > .25$)] (also **Bretherton**, 1969)

- **Lindzen** (1985) – wave saturation hypothesis: wave amplitudes adjust in response to the onset of convective/ small-scale shear Instability in regions where wave steepening occurs

- The E-P theorem in combination with the saturation hypothesis permits formulation of a simple wave theory basis for gravity-wave drag parameterization (Palmer et al., 1986; McFarlane, 1987)

Observing Campaigns

Appendix A from
R. B. Smith et al., JAS, 2016
(DEEPWAVE)
(**Talk by C. Kruse**)

- Sierra Wave Project from 1951 to 1955 (e.g., Grubišić and Lewis 2004).
- High-Altitude Clear Air Turbulence (HICAT) from 1964 to 1968 (Lilly et al. 1974).
- Colorado Lee Wave Experiment in 1970 (Lilly and Kennedy 1973).
- Wave Momentum Flux Experiment (WAMFLEX) in 1973 (Lilly et al. 1982).
- Appalachian Lee Wave Experiment in 1971 (Smith 1976).
- Alpine Experiment (ALPEX) in 1982 (e.g., Kim and Mahrt 1992).
- Airborne Arctic Stratosphere Expedition (AASE) in 1989 (Bacmeister et al. 1996).
- Pyrenees Experiment (PYREX) in 1990 (Hoinka 1984; Bougeault et al. 1997).
- Mesocale Alpine Experiment (MAP) in 1999 (e.g., Smith and Broad 2003; Doyle and Smith 2003; Smith et al. 2007).
- T-REX in 2006 (e.g., Smith et al. 2008; Doyle et al. 2011, Wroblewski et al. 2010).
- Stratosphere–Troposphere Analysis of Regional Transport 2008 (START08) (Zhang et al. 2015).
- Gravity Wave Life Cycle (GW-LCYCLE) in 2013 (Ehard et al. 2016).

Lilly and Kennedy (1973); Colorado Lee Wave Program

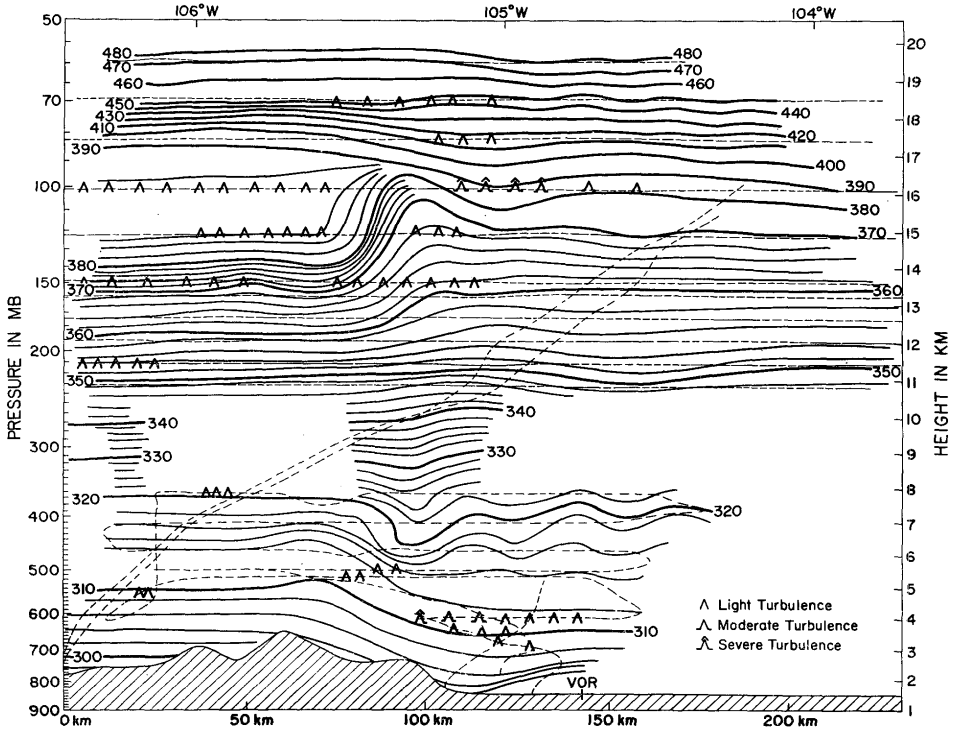

FIG. 1. Potential temperature cross section for 17 February 1970. Solid lines are isentropes (°K), dashed lines aircraft or balloon flight trajectories. The cross section is along a 275°–095° true azimuth line, crossing the Kremmling, Colo., and Denver VOR aircraft navigation stations.

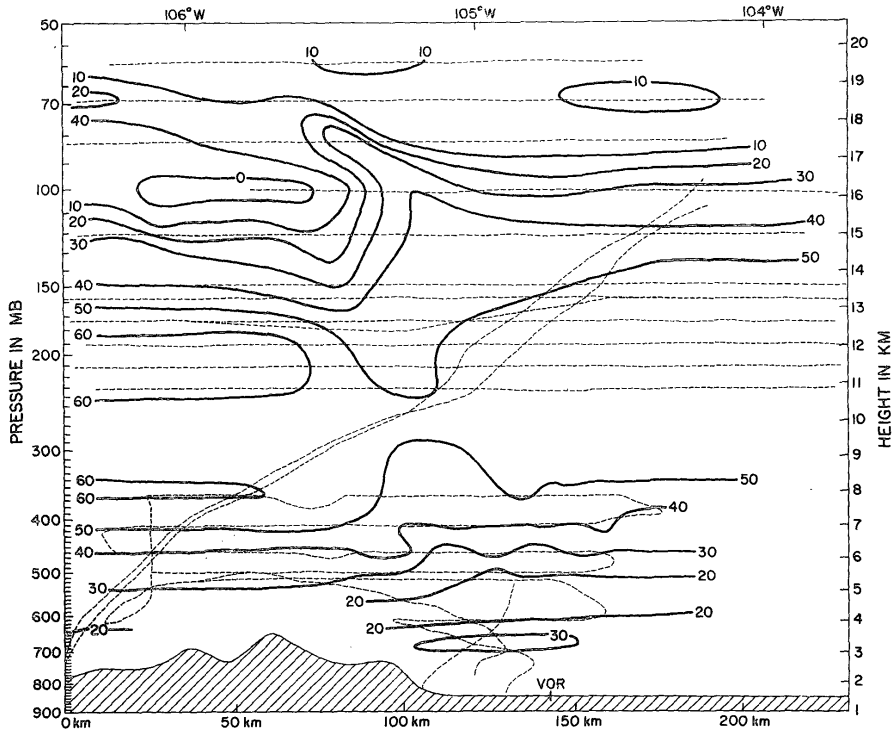

FIG. 2. Westerly wind component cross section for 17 February 1970. Isotachs are in m sec^{-1}.

Lilly and Kennedy (1973)

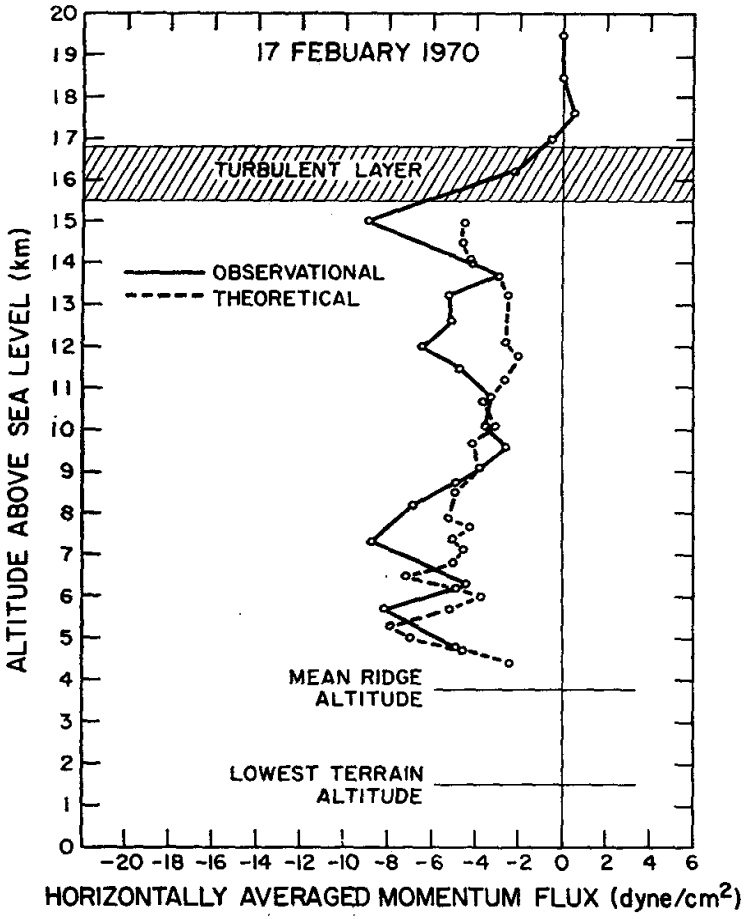

FIG. 14. Mean observed profile of momentum flux obtained by averaging the three curves shown in Fig. 13 (solid line). The computed profile of momentum flux derived from integration of Eqs. (5.7)–(5.9) is shown as the dashed line.

Lilly et al (1982)

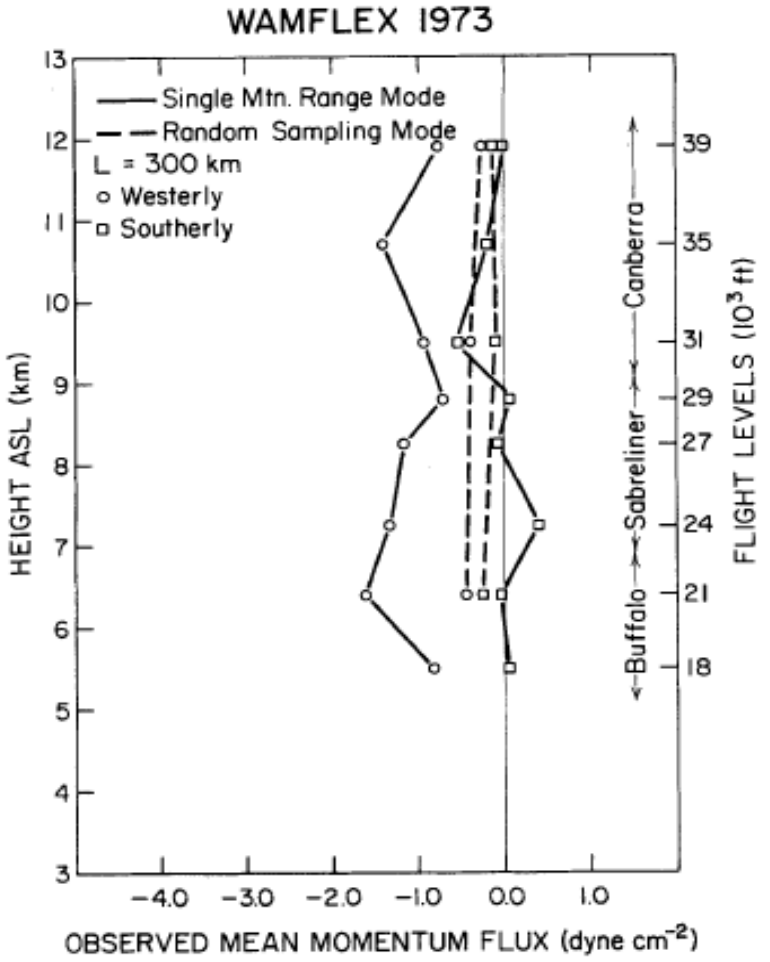

Figure 6. Profiles of westerly and southerly momentum flux averaged over all WAMFLEX flights. A horizontal distance, L, of 300 km is used. The aircraft altitude ranges on the right are approximate since there was considerable overlapping.

Basic 2-D linear wave theory for flow over a bell-shaped ridge (Drazin and Su, 1975)

Quasi-steady vertically propagating waves close to hydrostatic balance In a stably stratified slowly varying (in space) mean flow U over a ridge of the form $h(x) = h_0 / [1 + (x/a)^2]$ such that

$$f/U << 1/a << N/U \qquad N^2 = \frac{g}{\bar{\theta}}\frac{\partial \bar{\theta}}{\partial z} > 0$$

Perturbation potential temperature and velocity components in terms of the stream line vertical displacement

$$w' = U\partial\delta/\partial x \qquad u' = -\frac{1}{\bar{\rho}}\frac{\partial}{\partial z}(\bar{\rho}U\delta) \qquad \theta' = -\delta\frac{\partial \bar{\theta}}{\partial z} \qquad \frac{\partial}{\partial z}\left[\frac{U^2}{\bar{\rho}}\frac{\partial}{\partial z}(\bar{\rho}\delta)\right] + N^2\delta = 0$$

$$\delta(x,0) = h(x) \rightarrow \quad \delta \cong \frac{A(z)}{1+(x/a)^2}\left[\cos\left(\int_0^z \frac{N}{U}dz'\right) - \frac{x}{a}\sin\left(\int_0^z \frac{N}{U}dz'\right)\right] \quad A(z) = h_0\left[\frac{(\bar{\rho}(0)N(0)U(0))}{\bar{\rho}NU}\right]^{1/2}$$

$$\tau = \frac{1}{L}\int_{-\infty}^{\infty}\bar{\rho}u'w'\,dx \cong -\mu\rho(0)N(0)U(0)h_0^2 = -\mu\bar{\rho}NUA^2 \qquad \mu = \pi/(4L) \qquad L>>a$$

Wave breaking: $\partial(\bar{\theta}+\theta')/\partial z \cong (1-\partial\delta/\partial z)\partial\bar{\theta}/\partial z$ Saturation condition: $\max\left|\partial\delta/\partial z\right| \cong NA/U \le 1$

Saturation control: at the breaking levels set $A = A_b = U/N$

=> $$-\frac{1}{\bar{\rho}}\partial\tau/\partial z = -2\mu\frac{U^3}{N}Max\left[\partial(\ln F)/\partial z, 0\right] \qquad F(z) = \frac{Nh_0}{U}\left[\frac{\bar{\rho}(0)N(0)U(0)}{\bar{\rho}NU}\right]^{1/2}$$

In mid latitudes the effective inverse Froude number typically decreases with height in the region below the tropospheric jet maxima but increases rapidly with height in the region above jet maxima.

The effective ridge height for wave emission, h_{eff}, is constrained to ensure that $F(0) < Fc$

Non-linearity of the lower boundary condition:

$$\delta(x, h(x)) = h(x)$$

$\Rightarrow$ critical overturning value $F_c < 1$
{Depending on the geometry of the ridge Smith, 1977, Lilly and Klemp, 1979; Laprise and Peltier, 1988}

For bell-shaped ridge Fc=.85 (Miles&Huppert, 1969)

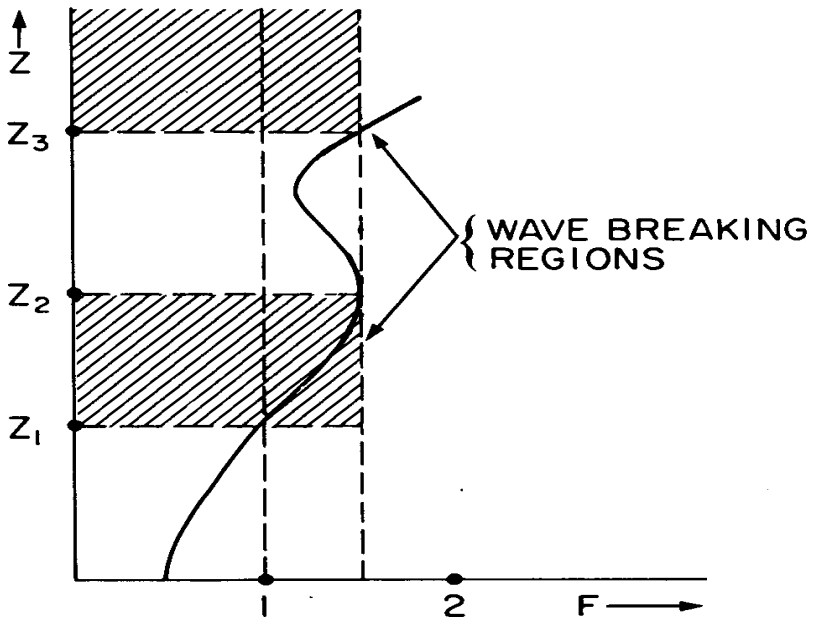

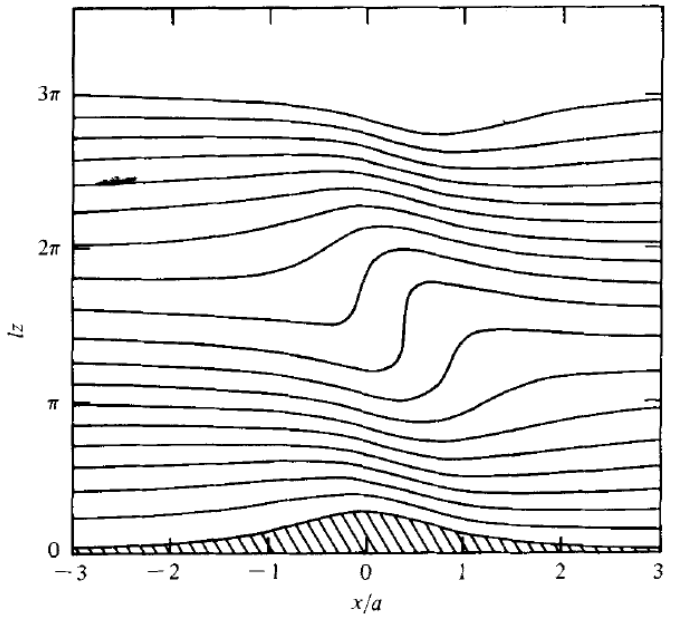

Lilly and Klemp, 1979

Palmer et al (1986)

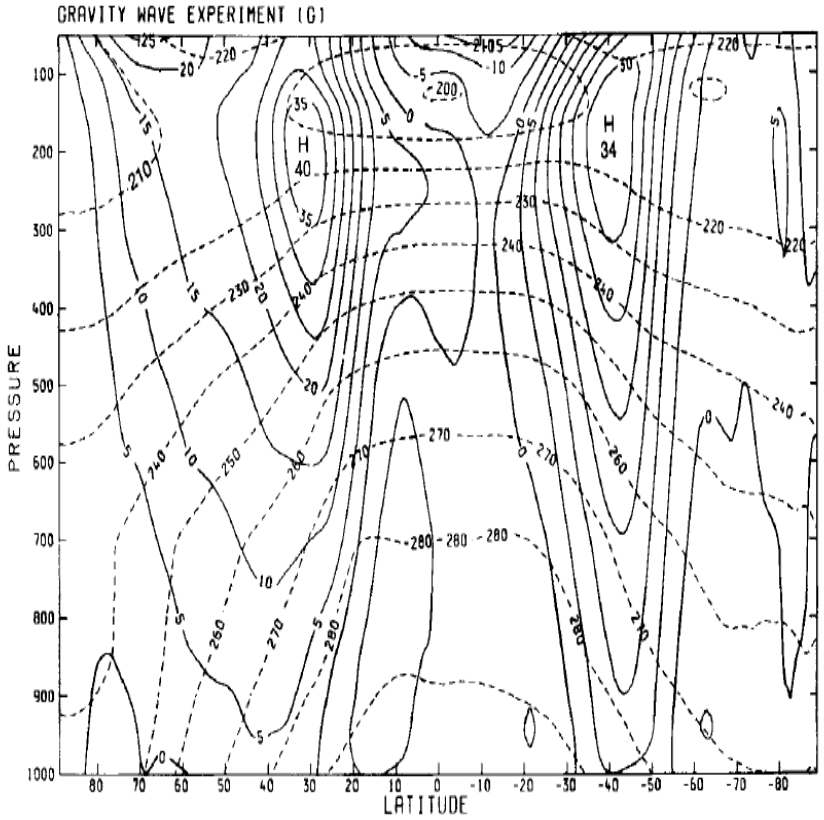

Figure 14. Zonal mean cross-section of zonal wind ($m\,s^{-1}$) and temperature (K) for experiment G.

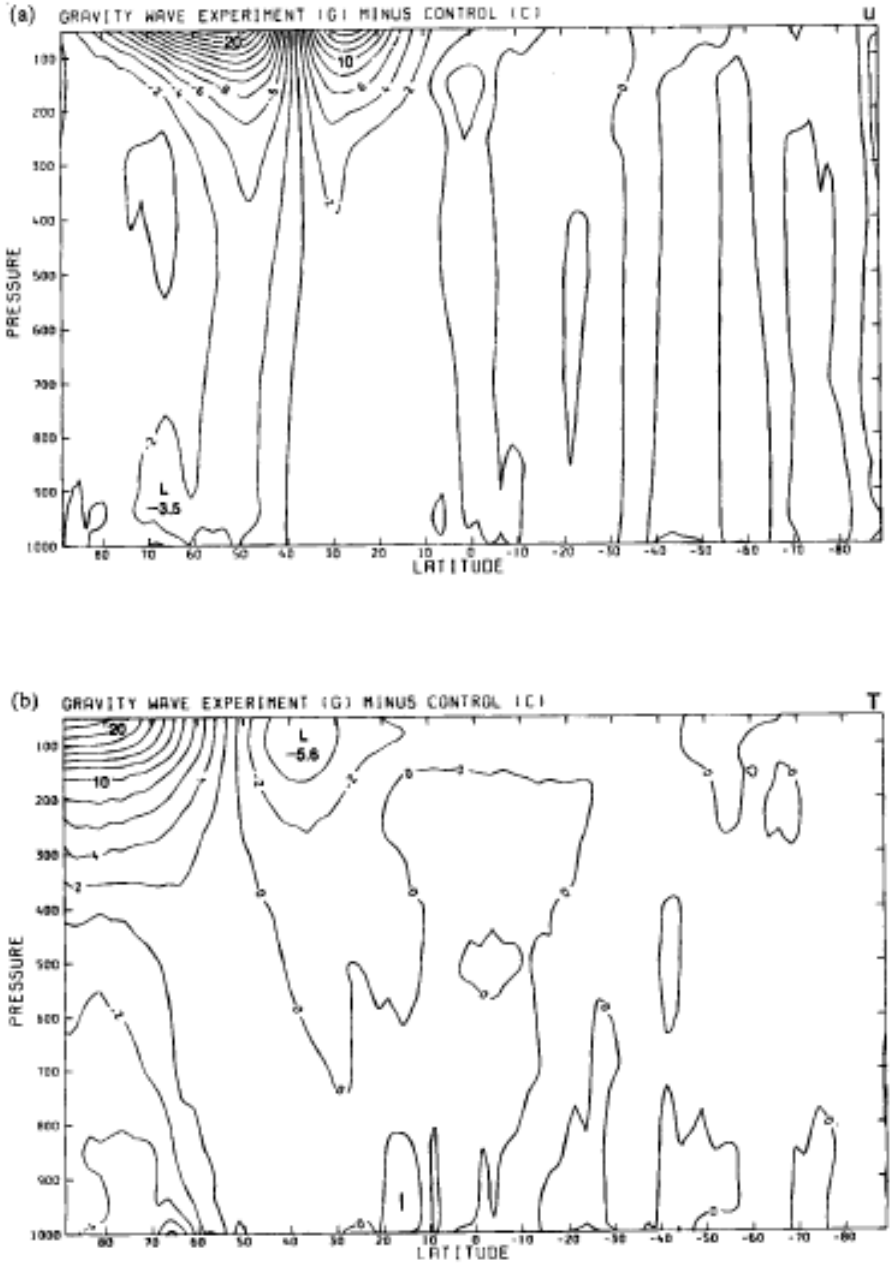

Figure 15. Zonal mean cross-sections of the differences in (a) zonal wind ($m\,s^{-1}$) and (b) temperature (K) for experiment G minus experiment C.

McFarlane (1987)

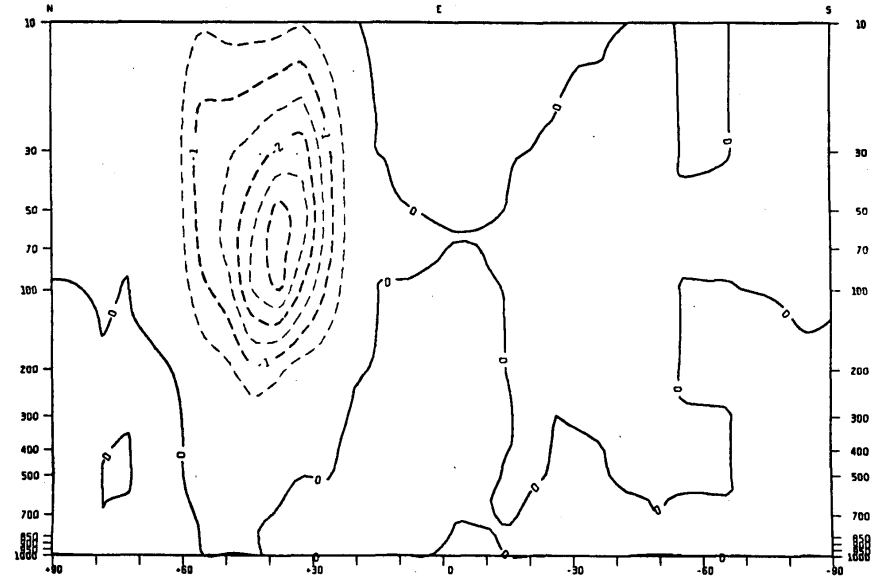

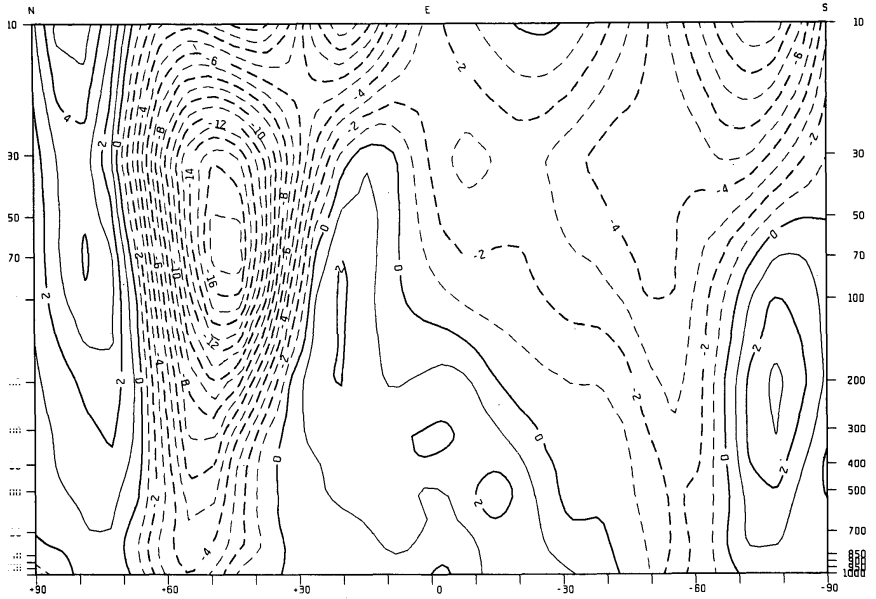

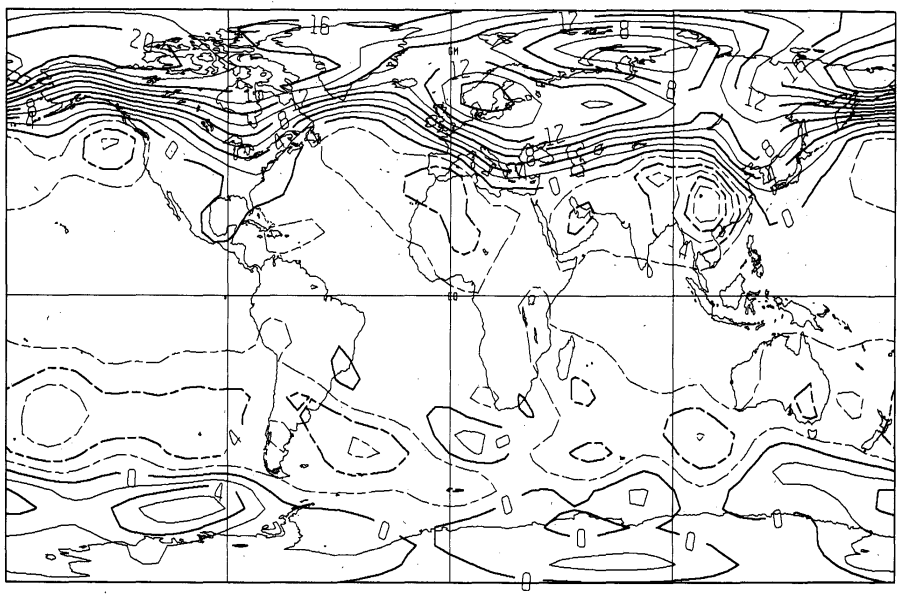

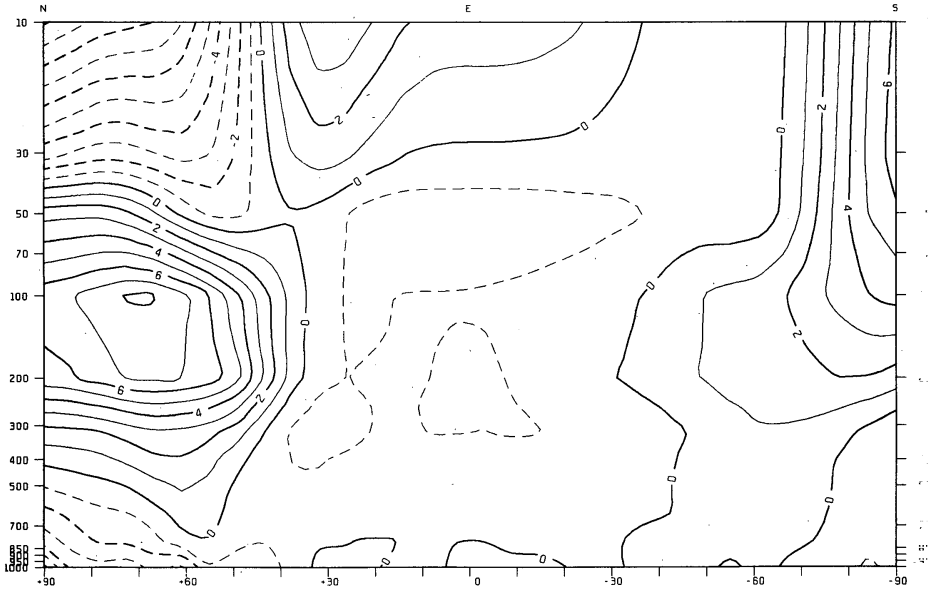

FIG. 19. Mean sea level pressure difference (WD-CONTROL). Contour interval: 2 mb.

TABLE 1. Intercomparison of selected sub-grid-scale orographic gravity wave parameterization schemes used mainly for the stratosphere and the troposphere. Here, $Fr \equiv Nh/U$, $Ri \equiv N^2/(\delta U/\delta z)^2$.

Designer/user(s) (year) and institution(s)	Drag at the reference level (τ_0)	Residual drag above the reference level (τ)	Sub-grid-scale orographic gravity wave amplitude (h)	Tuning coefficient ($k = m/\Delta x$)	Criterion for Lindzen's wave saturation
Boer et al. (1984) Atmospheric Environment Service (AES)/Canadian Climate Center (CCC)	$-\overline{k}\rho_0 N_0 U_0 h$	$\tau_0 \frac{z_2 - z}{z_2 - z_1}$; $z_2 \geqslant z > z_1$, when convectively unstable.	$\frac{9 \times 10^8 C_f^2}{1 + 4 \times 10^5 C_f^2}$; $C_f = \mathrm{Max}(C_D - 1.5 \times 10^{-3}, 0)$ C_D = Cressman drag coef.	Effective aspect ratio of the orographic features.	Saturation hypothesis not used.
Chouinard et al. (1986) AES/CCC	$-\overline{k}\rho_0 N_0 U_0 h$	$\left(\frac{\partial U}{\partial t}\right)_{\mathrm{GWD}} \propto -U^2 \mathrm{Max}\left\{1 - \frac{Fr_c^2}{Fr^2}, 0\right\}$	$2\sigma_h$ (σ_h: Standard deviation of sub-grid-scale orography.)	0.01	Saturation hypothesis not used, $Fr_c = \sqrt{0.5} = 0.71$
Palmer et al. (1986) United Kingdom Meteorological Office (UKMO)	$-k\rho_0 N_0 U_0 h^2$	$Fr_c^2 \frac{k\rho U^3}{N}$ if $Ri_m < Ri_c$; $Ri_m = Ri \frac{1 - Fr}{(1 + \sqrt{Ri}Fr)^2}$	$\mathrm{Min}(\sigma_h, 400\ \mathrm{m})$	$2.5 \times 10^{-5}\ \mathrm{m}^{-1}$	$Ri_c = 0.25$ $[Fr_c$ (for $Ri \gg 1$) $= \sqrt{0.69} = 0.83]$
McFarlane (1987) AES/CCC	$-k\rho_0 N_0 U_0 h^2$	$\left(\frac{\partial U}{\partial t}\right)_{\mathrm{GWD}} \propto -\frac{U^3}{N} \mathrm{Max}\left[\frac{d \ln Fr^2(z)}{dz}, 0\right]$	$\mathrm{Min}\left(2\sigma_h, \mathrm{Fr}_c \frac{U_0}{N_0}\right)$	$8.0 \times 10^{-6}\ \mathrm{m}^{-1}$	$Fr_c = \sqrt{0.5} = 0.71$
Pierrehumbert (1986) Geophysical Fluid Dynamics Laboratory (GFDL)/National Oceanic and Atmospheric Administration (NOAA)	$-k \frac{\rho_0 U_0^3}{N_0} G(Fr)$; $G(Fr) = \frac{Fr^2}{Fr^2 + 1}$ $\{Fr < Fr_c\}$ $\{=3 + 5(Fr - Fr_c)^2;\ Fr > Fr_c\}$	Decreasing linearly with height to zero.	σ_h	$\frac{1}{100\ \mathrm{km}} = 1.0 \times 10^{-5}\ \mathrm{m}^{-1}$	Saturation hypothesis not used, $\{Fr_c = 0.8\}$
Miller and Palmer (1986), Miller et al. (1989) European Centre for Medium-Range Weather Forecasts (ECMWF) and UKMO	$-k\rho_0 N_0 U_0 h^2$	$-k\rho NUh_i^2$; $h_i = \left[\frac{\Delta x \tau_{i+1}}{m(\rho NU)_i}\right]^{1/2}$ $Ri_m = Ri \frac{1 - Fr}{(1 + \sqrt{Ri}Fr)^2}$	$[\mathrm{Min}(\lvert\sigma_h\rvert^2, \lvert\sigma_h^*\rvert^2)]^{1/2}$; $\lvert\sigma_h^*\rvert^2 = \lvert\sigma_h\rvert^2_{\bar{a}}$, by MP, $\mathrm{Min}(\sigma_h, 400\ \mathrm{m})$ by MPS.	$2.5 \times 10^{-5}\ \mathrm{m}^{-1}$	$Ri_c = 0.25$
Stern et al. (1987) GFDL/NOAA	$-k \frac{\rho_0 U_0^3}{N_0} G(Fr)$; $G(Fr) = \frac{Fr^2}{Fr^2 + 1}$	$\tau_0 \left[1 - \frac{p - p_0}{p_T - p_0}\right]$; $p_T > p > p_0$	σ_h	$\left[\mathrm{Min}\left(\Delta x, \frac{3U_0}{N_0}\right)\right]^{-1}$	Saturation hypothesis not used.
McFarlane et al. (1987) CCC and Canadian Meteorological Centre (CMC)	$-k\rho_0 N_0 U_0 h^2$	$-k\rho NUh_i^2$; $h_i = \left\{\mathrm{Min}\left[\frac{(\rho NUh^2)_{i+1}}{(\rho NU)_i}, \left(\frac{UFr_c}{N}\right)_i^2\right]\right\}^{1/2}$	$\mathrm{Min}\left(2\sigma_h, Fr_c \frac{U_0}{N_0}\right)$	$\frac{1}{125\ \mathrm{km}} = 8.0 \times 10^{-6}\ \mathrm{m}^{-1}$	$Fr_c = 0.7$
Helfand et al. (1987) National Aeronautic and Space Administration (NASA)/ Goddard Space Flight Center (GSFC)	$-k\rho_0 N_0 U_0 h^2$	$-k\rho NUh^2$; $Fr_i^2 = \frac{\tau_{i+1} N_i}{k\rho_i U_i^2}$ $Ri_m = Ri(1 - Fr)$	$\mathrm{Min}\left(\mathrm{Min}(\sigma_h, 400\ \mathrm{m}), 0.85 \frac{U_0}{N_0}\right)$	$2.5 \times 10^{-5}\ \mathrm{m}^{-1}$	$Ri_c = 0.25$ $\left[Fr_c = 1 - \frac{1}{4Ri}\right]$
Alpert et al. (1988) National Meteorological Center (NMC)/National Weather Service/NOAA	$-k \frac{\rho_0 U_0^3}{N_0} G(Fr)$; $G(Fr) = \frac{Fr^2}{Fr^2 + 1}$	$-k\rho NUh^2$; $Fr_i^2 = \frac{\tau_{i+1} N_i}{k\rho_i U_i^2}$ $Ri_m = Ri(1 - Fr)$	σ_h	$\frac{1}{100\ \mathrm{km}} = 1.0 \times 10^{-5}\ \mathrm{m}^{-1}$	$Ri_c = 0.25$ $\left[Fr_c = 1 - \frac{1}{4Ri}\right]$
Stern and Pierrehumbert (1988) GFDL	$-k \frac{\rho_0 U_0^3}{N_0} G(Fr)$; $G(Fr) = \frac{Fr^2}{Fr^2 + 1}$	$\tau_{\mathrm{sat}} = -k\rho U^2 DG$; $D^{-2} = \frac{N^2}{U^2} - \frac{U_{zz}}{U}$ or $= \tau_0 \left[1 - \frac{p - p_0}{p_T - p_0}\right]$	σ_h	$\frac{1}{100\ \mathrm{km}} = 1.0 \times 10^{-5}\ \mathrm{m}^{-1}$	$\tau \geqslant \tau_{\mathrm{sat}}$ or no saturation hypothesis.
Iwasaki et al. (1989) Japanese Meteorological Agency	$-k\rho_0 N_0 U_0 h^2$	$-k_A \rho NUh^2$ $-k_B(\sigma - 0.3)^2$; $\sigma \equiv \frac{p}{p_s} > 0.3$	$\mathrm{Min}\left(\sigma_h, 0.5 Fr_c \frac{U_0}{N_0}\right)$	$2.0 \times 10^{-5}\ \mathrm{m}^{-1}$ for k_A $5.0 \times 10^{-5}\ \mathrm{m}^{-1}$ for k_B	$Fr_c = 1.0$
Surgi (1989) University of Miami	$-k\rho_0 N_m U_0 h^2$; $N_m = \sqrt{1 - \epsilon} N_d$ $(0 < \epsilon < 0.3)$	$-k\rho N_m U h_i^2$; $h_i = \left[\frac{\Delta x \tau_{i+1}}{m(\rho N_m U)_i}\right]^{1/2}$ $Ri_m = Ri \frac{1 - Fr}{(1 + \sqrt{Ri}Fr)^2}$	$\mathrm{Min}(\sigma_h, 400\ \mathrm{m})$	$2.5 \times 10^{-5}\ \mathrm{m}^{-1}$	$Ri_c = 0.25$
Hayashi et al. (1992) GFDL/NOAA	$-k\rho_0 N_0 U_0 h^2$	$\tau_0 \frac{\sigma - \sigma_c}{1 - \sigma_c}$; $\sigma_c \ll \sigma \leqslant 1$	σ_h	$2.2 \times 10^{-5}\ \mathrm{m}^{-1}$	Saturation hypothesis not used.
A test scheme, constructed following Pierrehumbert (1986) and Miller and Palmer (1986)	$-\frac{m}{\Delta x} \frac{\rho_0 U_0^3}{N_0} G(Fr)$; $G(Fr) = \frac{Fr^2}{Fr^2 + 1}$	$-k\rho NUh_i^2$; $h_i = \left[\frac{\Delta x \tau_{i+1}}{m(\rho NU)_i}\right]^{1/2}$ $Ri_m = Ri \frac{1 - Fr}{(1 + \sqrt{Ri}Fr)^2}$	σ_h	$\frac{\Delta x}{L_m}$	$Ri_c = 0.25$
A revised scheme constructed in the present study	$-E \frac{m}{\Delta x} \frac{\rho_0 U_0^3}{N_0} \frac{Fr^2}{Fr^2 + C_G/\mathrm{OC}}$; $E = (\mathrm{OA} + 2)^{C_E Fr_0/Fr_c}$	$-k\rho NUh_i^2$; $h_i = \left[\frac{\Delta x \tau_{i+1}}{m(\rho NU)_i}\right]^{1/2}$ $Ri_m = Ri \frac{1 - Fr}{(1 + \sqrt{Ri}Fr)^2}$ $\frac{\tau_i}{\tau_{i+1}} = \mathrm{Min}\left[C_l \frac{l_i^2}{l_{i+1}^2}, 1\right]$; $\mathrm{OA} > 0$, $z < z_T$.	σ_h	$C_m \left[1 + \frac{\Sigma L_h}{\Delta x}\right]^{\mathrm{OA}+1}$; $C_m = 3.3 \times 10^{-5}\ \mathrm{m}^{-1}$, $C_E = 0.8$, $C_G = 0.5$, $C_l = 1$, $z_T \approx 10$ km	$Ri_c = 0.25$ $Fr_c = 1.0$

Kim and Arakawa,1995

}←

But occasionally downslope wind storms with associated high-drag states occur. (Lilly (1978)

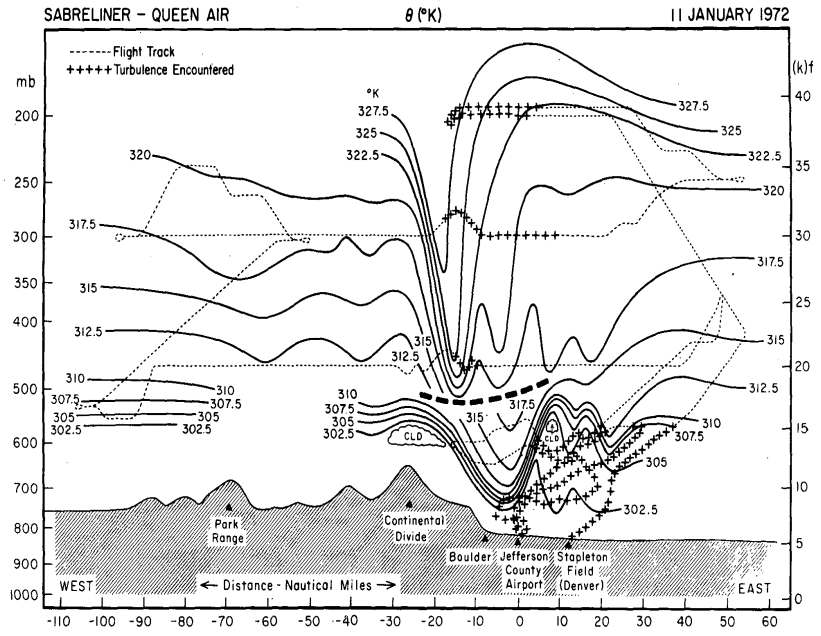

FIG. 7. Analysis of the potential temperature field (solid lines) from aircraft flight data and sondes taken on 11 January 1972. The dashed lines show aircraft track, with periods of significant turbulence shown by pluses. The heavy dashed line separates data taken by the Queen Air at lower levels before 2200 GMT from that taken by the Sabreliner in the middle and upper troposphere after 0000 GMT (12 January). The aircraft flight tracks were made along an approximate 130°–310° azimuth, but the distances shown are along the east-west projection of those tracks.

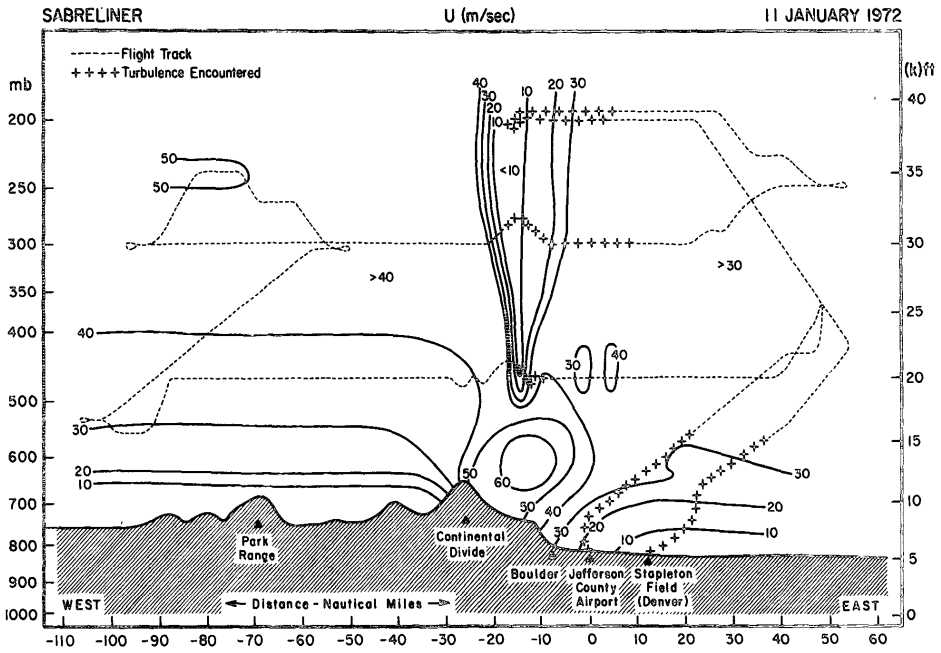

FIG. 9. Analysis of westerly wind component (m s^{-1}) on 11 January 1972, made from Sabreliner and sonde data only. The analysis below 470 mb over the eastern slope was deduced from assumptions indicated in the text.

Estimated average wave momentum flux from aircraft flight legs at 20,000 and 30,000 ft : **47 dynes/cm²** . (Klemp and Lilly, 1978)

Blocking and Downslope Wind Storms theory and modelling
[reviews by *R. B. Smith*, Advances in Geophysics (31), 1989;
M. Teixeira, Front. Phys., 2014]

Klemp and Lilly : (1975) - *Resonant amplification of linear waves in the presence of favourable flow and stratification - an inversion near mountain top and an upstream wind profile such that the waves reverse phase between the surface and tropopause.*

Peltier &Clark: (1979) – *Strong amplification for more homogeneous upstream conditions in association with development of super-critical overturning of streamlines within a vertical wave length above the ridge. Trapping and amplification of an internal wave beneath the wave-induced level of super-critical steepening . (also **Clark & Peltier**, 1984)*

Pierrehumbert and Wyman: (1985): *Relationships between wave breaking, downstream acceleration and propagation of upstream modes generated by when the inverse Froude number (Nh_m/U) is sufficiently large.*

Smith : (1985) – *Steady-state hydrostatic internal hydraulic theory. Key idealization: assumption of a dividing streamline above which the flow is quiescent. High drag transition states may develop for a discrete set of values of the height of this streamline.*

Bacmeister and Pierrehumbert: (1987) – *critical examination of C&P and Smith theories, partial support of the hydraulic theory of Smith when wave breaking occurs*

[***Later developments***: **Laprise & Peltier**, 1989; **Scinocca & Peltier**, 1989, **Garner**, 1995]

- 3-D modelling studies (e.g. **Miranda and James**, 1992, **Olafsson and Bougeault**, 1996,1997, **Schar and Durran**, 1997) and laboratory studies (**Baines**, 1995) ➔ additional effects including:

- *development and shedding of lee vortices (**Olafsson & Bougeault**, 1996; **Schar & Durran**, 1997, **Bauer et al**., 2000) (**Baines**, 1995, ch.6)*

- *sensitivity to the presence of surface friction and effects of rotation on drag (**Olafsson and Bougeault**, 1997, **Shutts**, 1998, **Wells** et al.,2005) lift forces(**Smith**,1979; **Bannon**, 1986; **Lott**1999; **Wells** et.al., 2005)*

- *enhanced deflection of the low-level flow around ridges with the onset of high-drag states (**Epifanio and Durran**, 200*

Miranda and James:

- Fluctuating High Drag Regime
- Low drag --> potential flow for Froude numbers < <.1

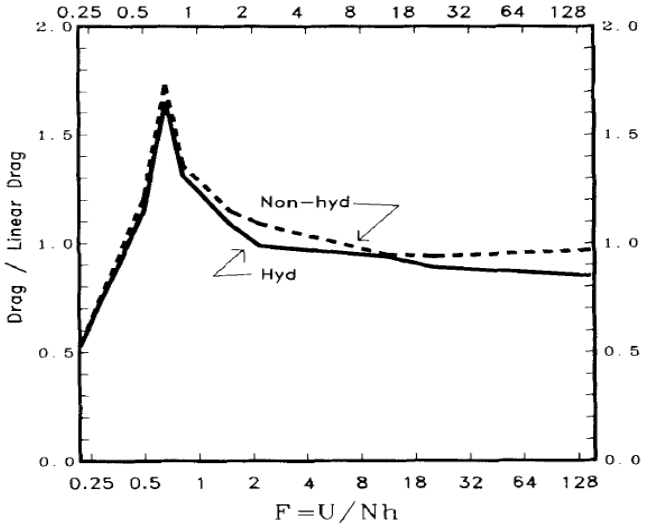

Effects of Earth Rotation

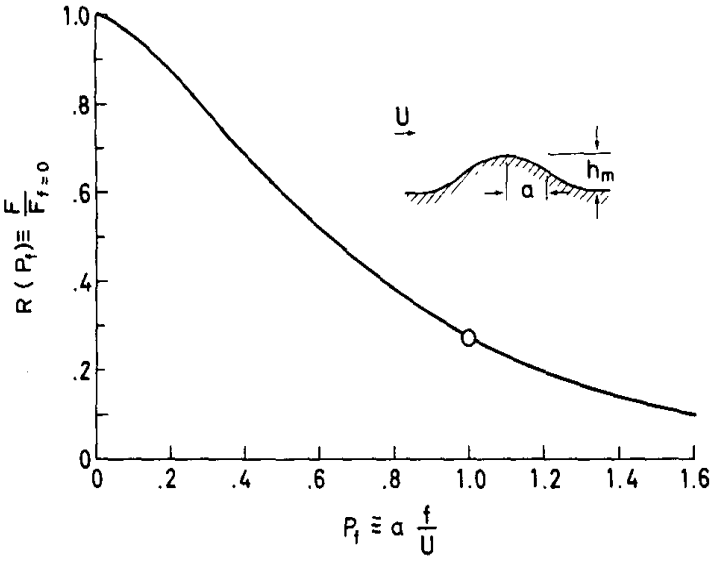

Linear theory (Smith ,1979)

Bretherton, 1969 (2-D linear) theory:
particle displacement in the y direction η'

$$v' = U\partial\eta'/\partial x$$

$$\frac{\partial}{\partial z}[\bar{\rho}w'(u' - f\eta')] = 0$$

$$D = \int_{-\infty}^{\infty} h\frac{\partial p}{\partial x}dx = \bar{\rho}\int_{-\infty}^{\infty}[(u' - f\eta')w']dx$$

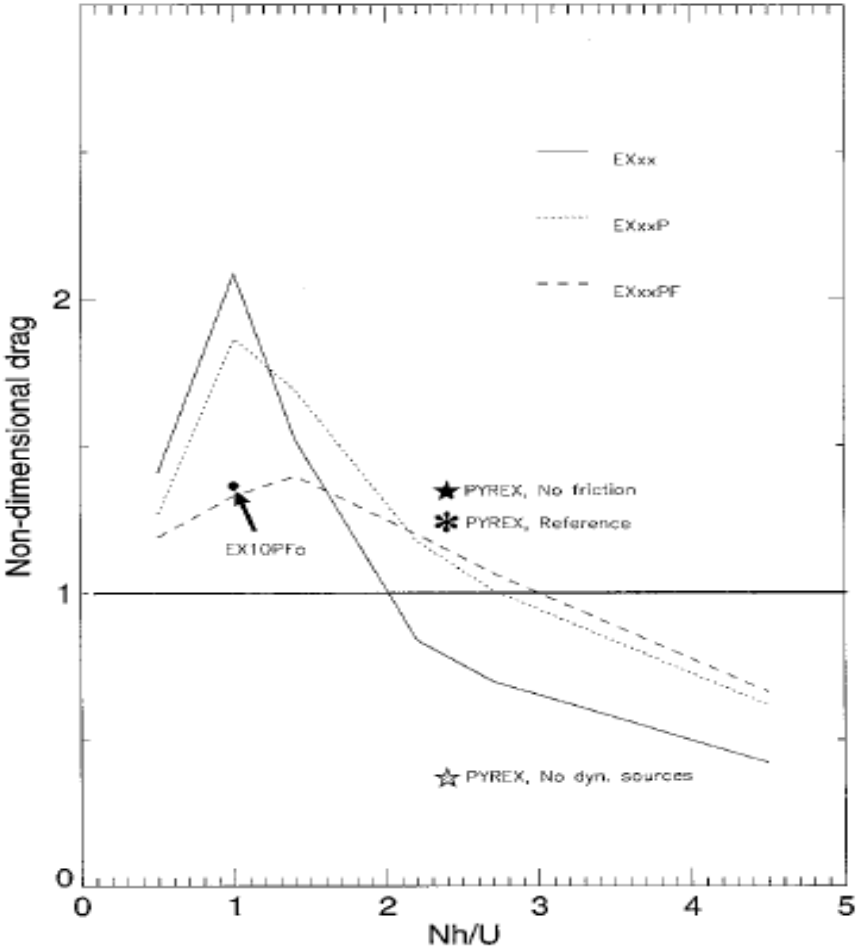

FIG. 4. Nondimensional drag along the central cross section as a function of Nh/U, for the $R = 5$ mountain. The simulated values of the drag in a cross section along the central part of the Pyrénées on 16.11.90 at 0900 UTC are also given ($\bar{N}h/\bar{U} = 2.4$). The drag is normalized with Eq. (9).

Olafsson & Bougeault
1997

Drag Regimes

Lott and Miller, 1997

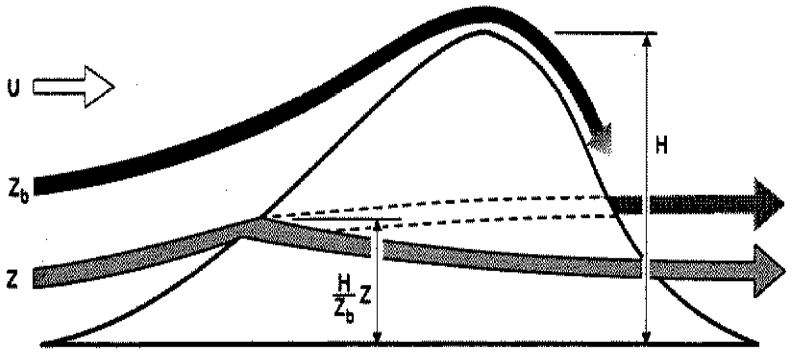

Figure 1. Schematic representation of the low-level flow behaviour parametrized in the new scheme details.

Miranda and James Ex. FR3

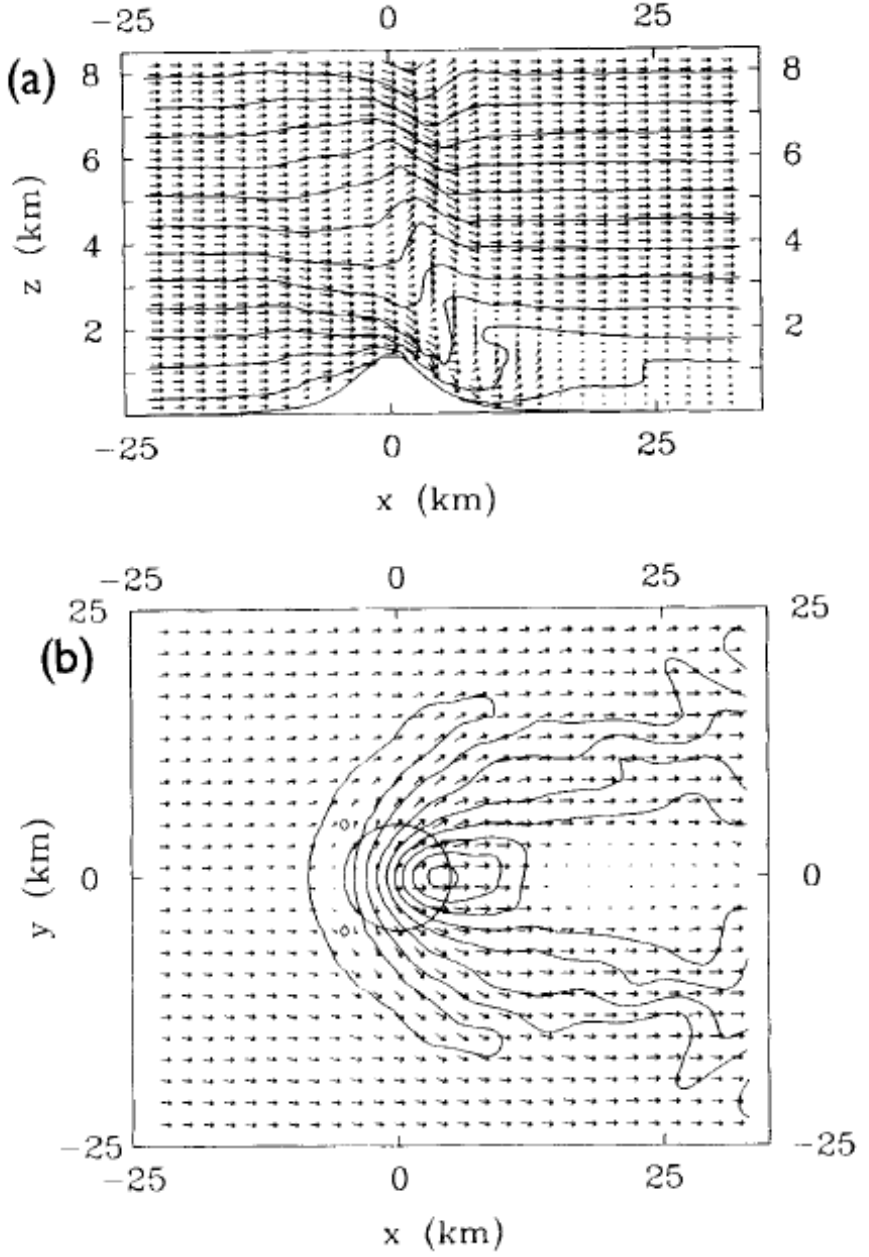

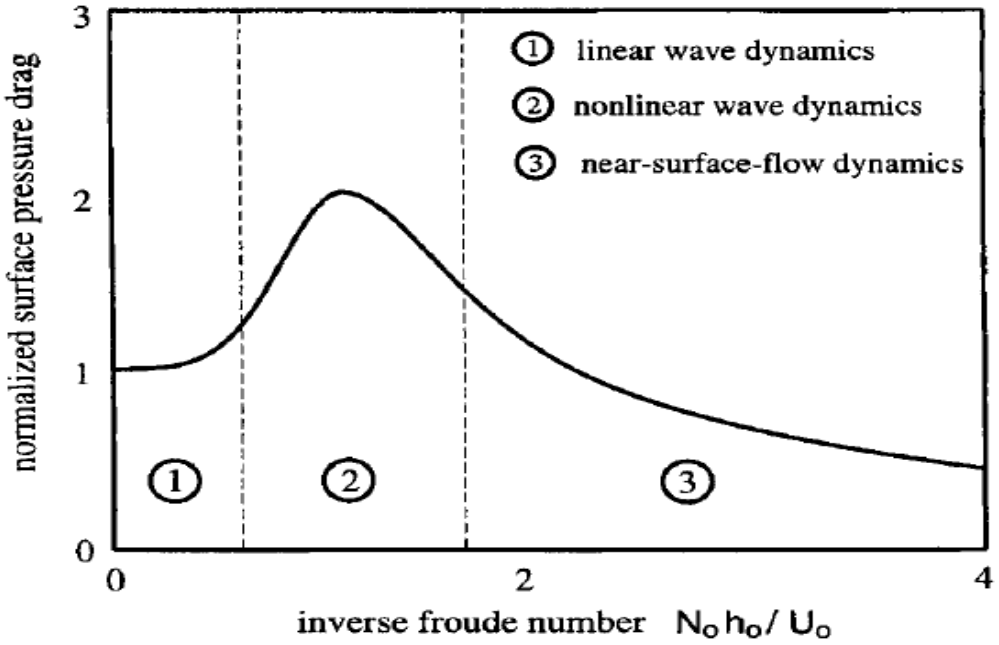

Scinocca and McFarlane, 2000

Regime 1: The Wave Field: One or more waves represented by simple wave parameterizations. For isolated ridges, (e.g. elliptical) at least two waves may be needed (Hines, 1988) to capture effects that are missing or poorly represented by single-wave schemes. (see also Garner, 2005)

Regime2: Wave drag + form drag (Lott & Miller, Scinocca&McFarlane, Garner, 2005) + nonlinear (downslope) drag enhancement (Scinocca&McFarlane)

Regime3: Predominantly form drag

Phillips (1984): 3-D Isolated elliptical ridges: $h(x',y') = h_0 \Big/ \left[1 + (x'/a)^2 + (y'/b)^2\right]$

Linear gravity wave pressure drag force due to N ridges in an area L^2 has components parallel$_{(1)}$ and perpendicular $_{(2)}$ to the upstream flow:

$$F^{(p)}_{(1,2)}(\gamma,\psi) = \frac{N}{2L^2}\rho_0 N_0 U_0 h_0^2 bG \int_{-\pi/2}^{\pi/2} A_{(1,2)}(\phi;\gamma,\psi)\,d\phi$$

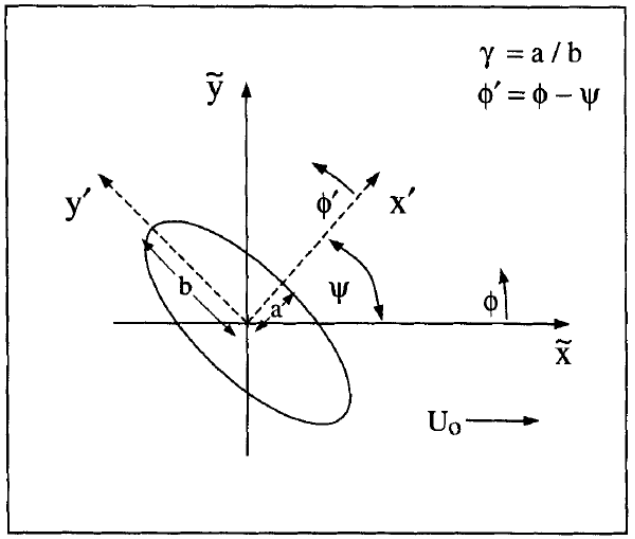

(Scinocca and McFarlane)

Basic forms of surface drag components :

Wave drag:

$$\vec{\tau}_{free} = \vec{\tau}_{linear} Min(F_c^2 / F^2(0), 1)$$

$$\vec{\tau}_d = [1 + \beta(F)]\vec{\tau}_{linear} - \vec{\tau}_{free}; F_c \le F \le 3F_c$$ (downslope)

Form drag:

$$\vec{\tau}_b = -\frac{1}{2}\frac{N_0}{L^2} C l_b h_b \vec{U}(0)\left|\vec{U}(0)\right|$$

Scinocca & McFarlane
C=effective drag coefficient

[Simulated from Olafsson & Bougeault]

{Note: cases for which Nh/U>>2 frequently have small values of U}

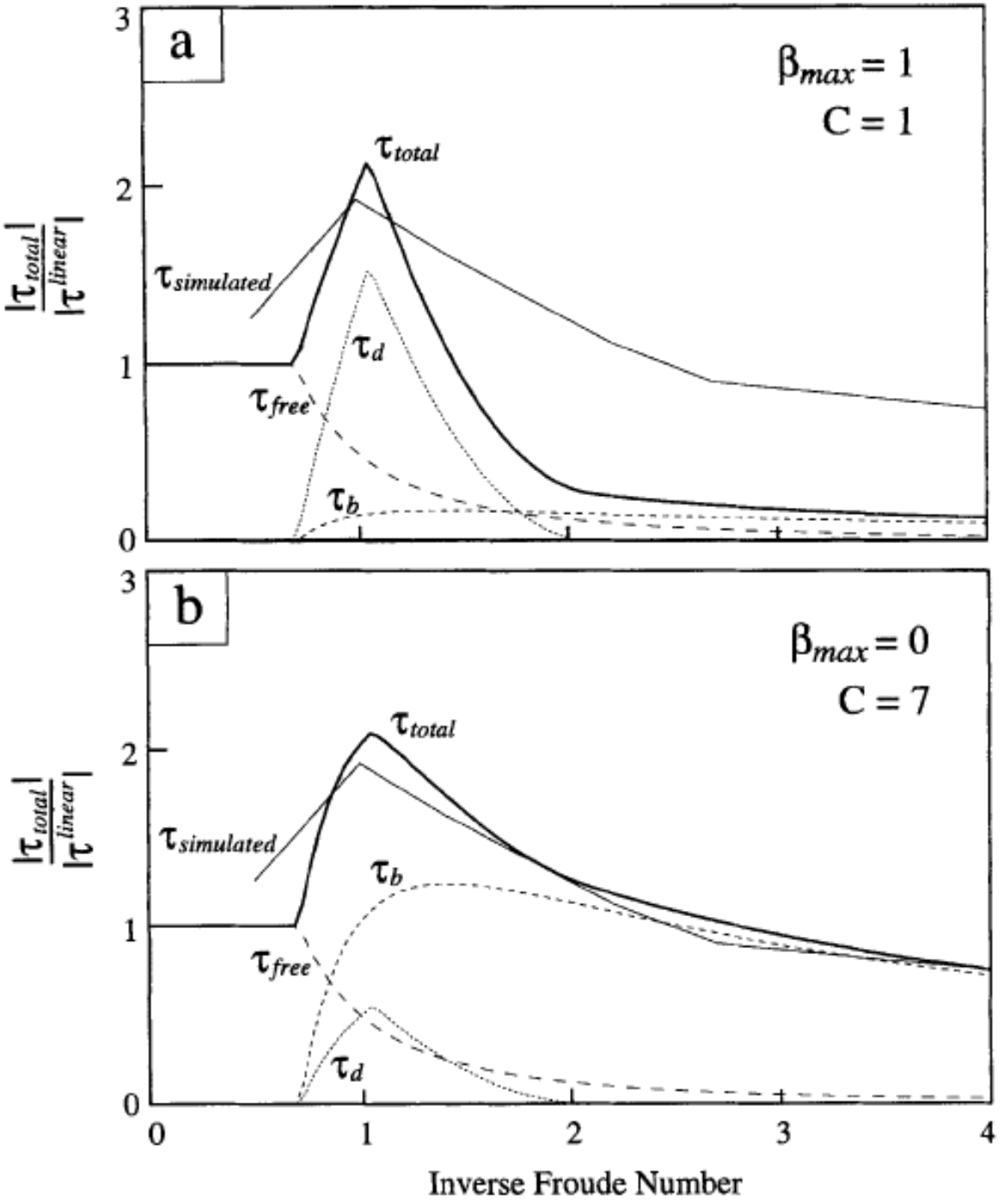

Scinocca and McFarlane, 2000

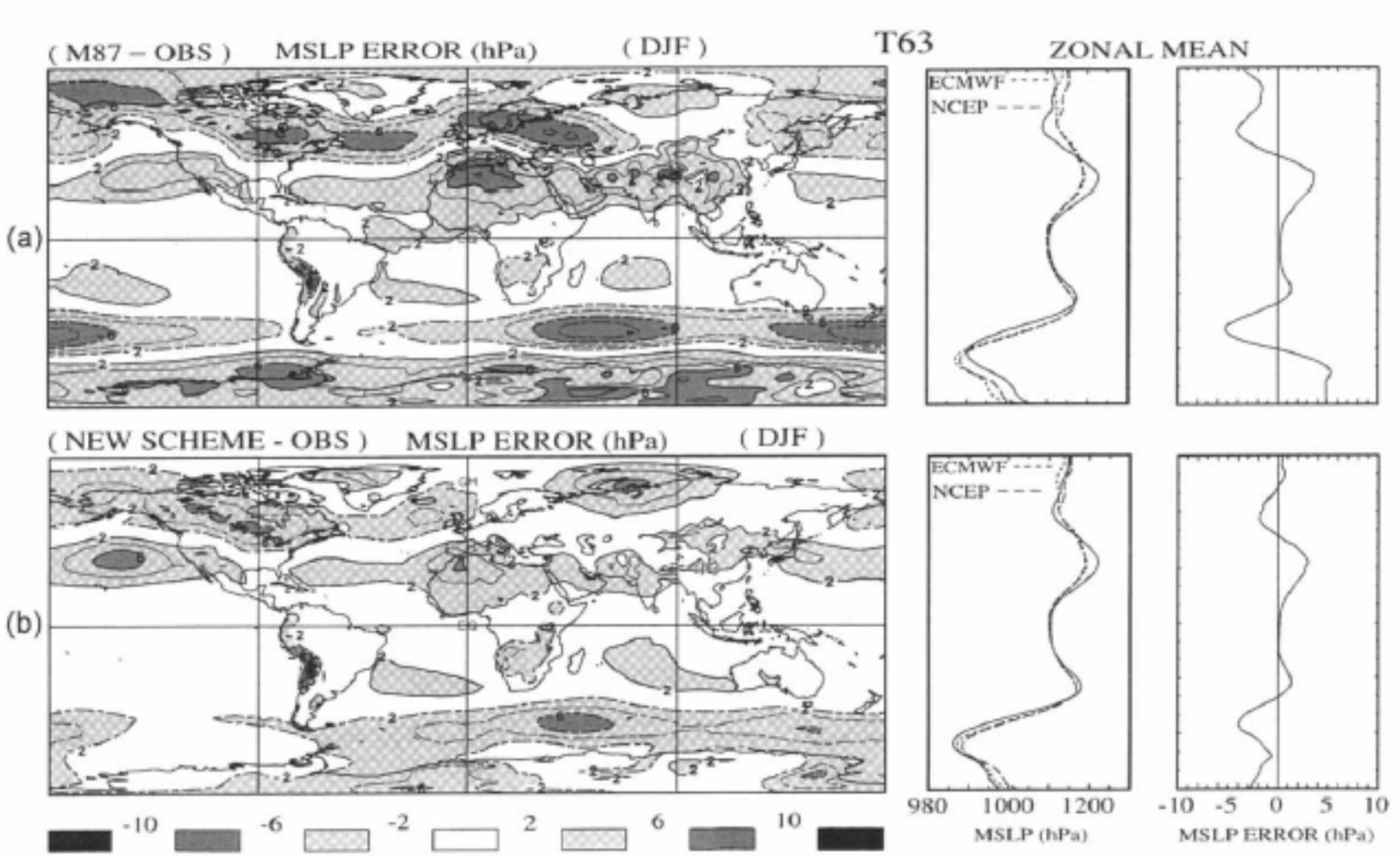

Scinocca and McFarlane, 2000

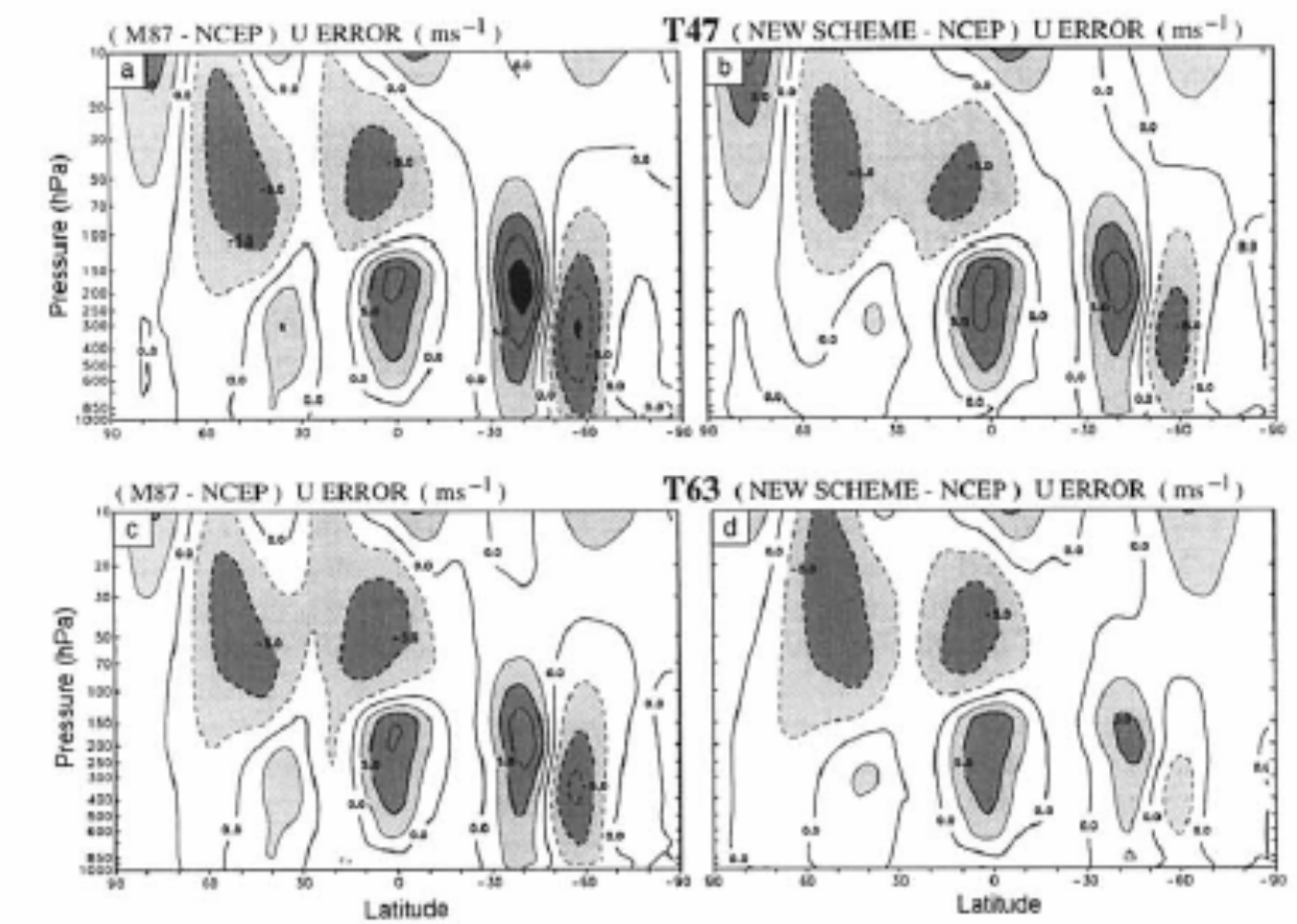

Figure 11. Latitude–height plots of December–January–February (DJF) zonal-mean zonal-wind errors from 5-year climate runs using (a) and (c) M87 and (b) and (d) the new scheme at horizontal resolutions of (a) and (b) T47 and (c) and (d) T63. The contour interval is 2.5 m s^{-1}, negative values are shown dashed, and darker shading indicates errors of larger magnitude.

Issues

- Dynamics of downslope wind storms and associated non-linear high drag states

are still an active field of study - frequency of occurrence, dominant mechanisms among the many that contribute , "best" formulation for the vertical structure of associated drag effects is still an open question. "Regime" definitions, role of mountain geometry,… (*Bauer et al. 2000*). (**Talks by U. Achatz; S. Garner; S. Vosper; J. Bacmeister**).

- Drag associated with trapped lee-wave systems (Bretherton, 1969; Smith, 1976; Lott, 1998, 2016; Broad, 2002) - ignored in parameterizations**. (Talk by M. Teixeira)**

- On larger (resolved) scales, non-zonal effects on both parameterized and resolved processes

- Interplay between parameterized and resolved contributions to mountain torques in the angular momentum budget (not additive - substantial compensation occurs: *Boer and Lazare, 1988….*) (**Talk by A. van Niekerk**)
- Coupling of gravity waves and planetary waves in the middle atmosphere: partial compensation between resolved planetary wave driving of the zonal mean flow and GWD (McLandress and McFarlane, 1993; A.K. Smith, 1996, 1997, Sigmond and Scinocca, 2010, Cohen et al. 2013, Sigmond and Shepherd, 2014). (**Talk by J. Scinocca**)

- Coupling with other processes e.g. turbulent transfer in the boundary layer and the free atmosphere; turbulent form drag (*Beljaars et al*, 2004);

[*energy conservation constraints in GCMs (Boville and Bretherton, 2003, Williamson et al., 2016) often assume a local balance between production and dissipation of turbulence*].

Models may include a budget of turbulent kinetic energy of a typical form:

$$\bar{\rho}\frac{D\mathrm{e}}{Dt}+\frac{\partial}{\partial z}\left(\overline{\bar{\rho}w'\vec{V}'\bullet\vec{V}'}/2+\overline{w'p'}\right)=-\overline{\bar{\rho}w'\vec{V}'}\bullet\frac{\partial\vec{\bar{V}}}{\partial z}+\bar{\rho}\overline{w'B}+S_D-\bar{\mathcal{D}}$$

$\mathrm{e}=\overline{\vec{V}'\bullet\vec{V}'}/2$: Turbulent kinetic energy

S_D : TKE source due to other drag/momentum transfer processes

$\bar{\mathcal{D}}=\bar{\rho}c_d\mathrm{e}^{3/2}/l_d$: TKE dissipation

Boville and Bretherton, 2003; **Williamson et al.**, 2016 in the context of energy conservation in CAM: Ignore TKE tendency and transport terms on the LHS

=> TKE net production=dissipation => heating